JOURNAL OF GEOPHYSICAL RESEARCH, VOL. 103, NO. B9, PAGES 21,201–21,213, SEPTEMBER 10, 1998

Upper mantle seismic velocity structure beneath Tanzania, east Africa: Implications for the stability of cratonic lithosphere

Jeroen Ritsema,[1,2] Andrew A. Nyblade,[3] Thomas J. Owens,[1]
Charles A. Langston,[3] and John C. VanDecar[4]

Abstract. The assertion of cratonic stability put forward in the model for deep continental structure can be tested by examining upper mantle structure beneath the Tanzania Craton, which lies within a tectonically active region in east Africa. Tomographic inversions of about 1200 teleseismic P and S travel times indicate that high-velocity lithosphere beneath the Tanzania Craton extends to a depth of at least 200 km and possibly to 300 or 350 km. Based on the thickness of mantle lithosphere beneath Archean cratons elsewhere, it appears that the mantle lithosphere of the Tanzania Craton has not been extensively disrupted by the Cenozoic tectonism in east Africa, thus corroborating the assertion of cratonic stability in the model for deep continental structure. The presence of thick, high-velocity structure beneath the Tanzania Craton implies relatively low temperatures within the cratonic mantle lithosphere, consistent with relatively low surface heat flow. The thick cratonic keel is surrounded by low seismic velocity regions beneath the east African rifts that extend to depths below 400 km. Our models show a shear velocity contrast between the cratonic lithosphere and the uppermost mantle beneath the eastern branch of the rift system of about 5% to 6%, but from resolution experiments we infer that this contrast could be underestimated by as much as a factor of 1.5. We attribute about half of this velocity contrast to the depleted composition of the cratonic keel and the other half to thermal alteration of upper mantle beneath the rifts. Low-density structures that may be required to provide buoyant support for the elevation of the Tanzania Craton must reside at depths greater than about 300–350 km.

1. Introduction

The existence of thick (> 200 km), petrologically depleted mantle lithosphere beneath ancient continental regions forms the basis of the model for deep continental structure [*Jordan*, 1978, 1988]. In this model, the lithospheric keels beneath cratons have resisted thermal erosion and entrainment in mantle convection for several billion years, and consequently, they are viewed as true islands of tectonic stability within a generally mobile and less stable lithosphere. Although evidence of cratonic disruption through tectonic processes does exist (e.g., the North American Craton during rifting of the North Atlantic Ocean and the Wyoming Craton during the Laramide Orogeny), opportunities to study the response of cratons to present-day tectonics are quite limited. However, an excellent, if not unique, setting to examine the relative strength of Archean lithosphere can be found in east Africa, where a number of Precambrian terrains lie within an area of Cenozoic tectonism.

The tectonic framework of east Africa is illustrated in Figure 1. The Archean Tanzania Craton lies in the center of the East African Plateau at a mean elevation of about 1000 m and is surrounded by the Proterozoic Mozambique, Ubendian, and Kibaran Belts. The 4000 km long Cenozoic rift system splits into two branches (the western and eastern branches) that traverse primarily through the mobile belts around the Tanzania Craton. The East African Plateau is part of the African Superswell, a large area of anomalous topography comprising the contiguous eastern and southern African plateaus and a region of elevated bathymetry in

[1]Department of Geological Sciences, University of South Carolina, Columbia.
[2]Now at Seismological Laboratory, California Institute of Technology, Pasadena.
[3]Department of Geosciences, The Pennsylvania State University, University Park.
[4]Department of Terrestrial Magnetism, Carnegie Institution of Washington, Washington, D.C.

Paper number 98JB01274.
0148-0227/98/98JB-01274$09.00

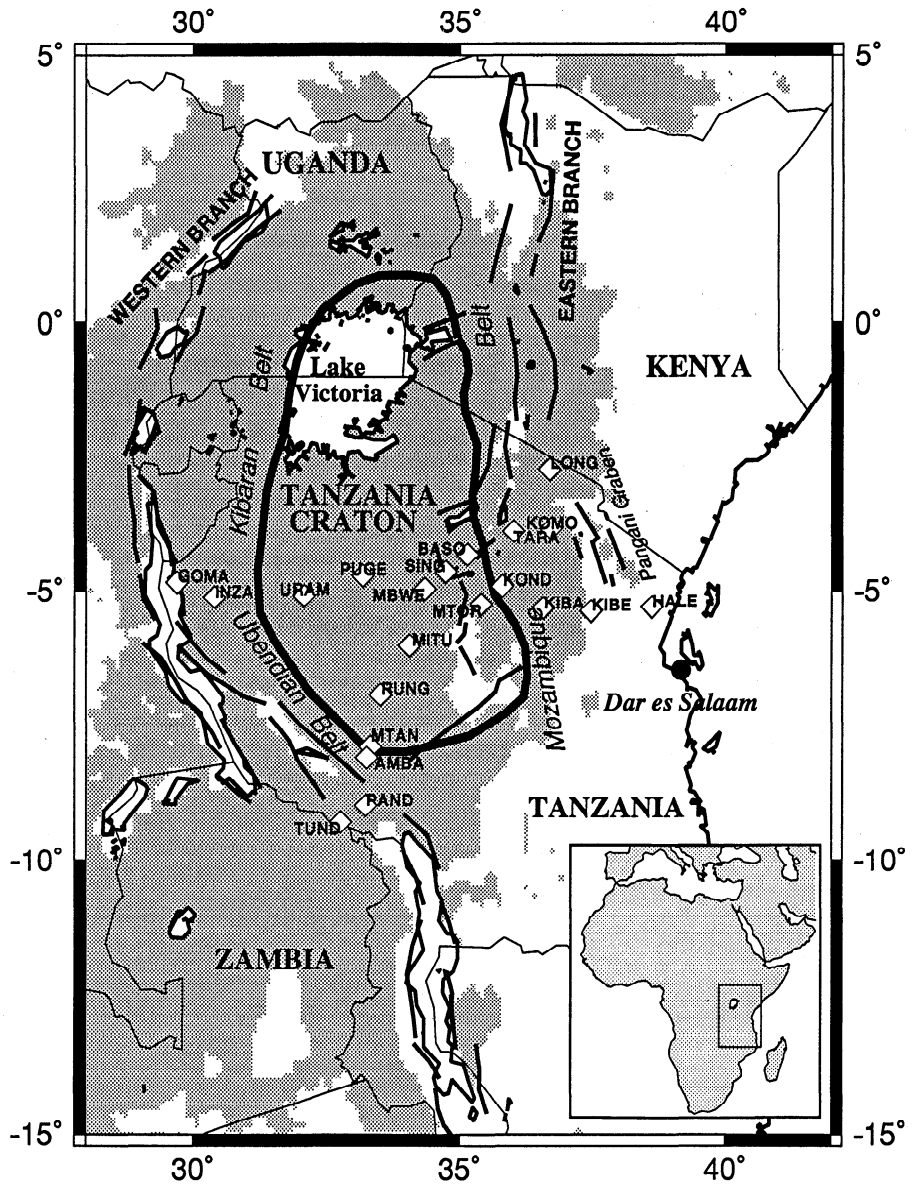

Figure 1. Schematic geologic map of east Africa showing the location of the Tanzania Craton (thick line), the surrounding rifted mobile belts, the major rift faults (intermediate lines), and international borders (thin lines). Regions shaded dark grey are higher than 1 km in elevation. Locations of the seismic station of the Tanzania Seismic Network are indicated by open diamonds.

the adjacent southeastern Atlantic Ocean [*Nyblade and Robinson*, 1994].

Geophysical studies of the eastern branch of the rift system in Kenya [e.g., *Prodehl et al.*, 1994, and references therein] and the western branch [*Nolet and Müller*, 1982] provide compelling evidence for extensive disruption of mantle lithosphere under the rifted mobile belts, presumably caused by upwelling hot (low density) asthenosphere replacing or modifying the mantle lithosphere. A plume source has been invoked by many authors for the upwelling material, as well as for the origin of the plateau uplift, since the amount of extension across east Africa is very small (~ 10–15 km).

The deep structure of the Tanzania Craton is not well constrained, and two competing end-member models have emerged from analyses of potential field observations. The first model (Figure 2a), derived from forward modeling of the Bouguer gravity anomaly across the East African Plateau, suggests that the Archean lithosphere has been extensively thinned and replaced by upwelling asthenosphere [e.g., *Girdler et al.*, 1969; *Wohlenberg*, 1975]. If this model is correct, then the assertion of cratonic stability described above would need to be reevaluated. The other end-member model (Figure 2b), which shows an undisturbed lithospheric keel beneath a stable craton, is largely inferred from the observation that heat flow from the Tanzania Craton is not elevated [*Nyblade et al.*, 1990; *Nyblade*, 1997], suggesting that the cratonic lithosphere has not been thermally perturbed. Since diamonds commonly form

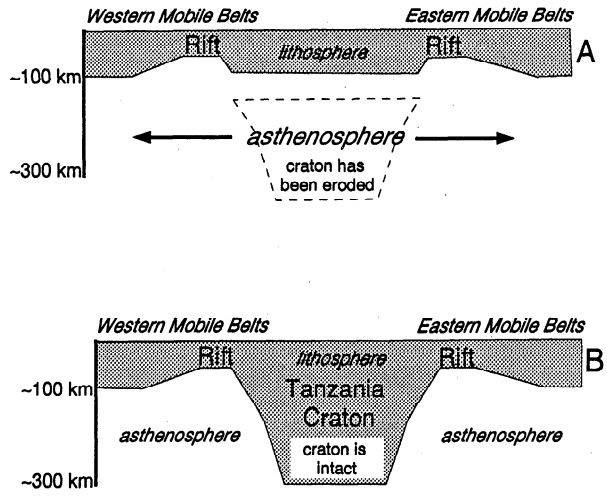

Figure 2. Vertical cross sections through end-member models of the Tanzania Craton and adjacent mobile belts. (a) Lithosphere of the Archean Tanzania Craton has been eroded and replaced by low-density asthenosphere. (b) Tanzania Craton is intact and has a lithosphere over 200 km thick.

at depths of 150–200 km and at relatively low temperatures [e.g., *Boyd et al.*, 1985; *Boyd and Gurney*, 1986], the presence of diamondiferous kimberlites in the Tanzania Craton supports this model. End-member model B is also supported by pressure-temperature estimates from mantle xenoliths collected from a Tertiary volcano along the eastern edge of the Tanzania Craton [*Chesley and Rudnick*, 1996; *Rudnick et al.*, 1994].

To refine models of the crust and upper mantle of the Tanzania Craton and the eastern and western branches of the East African Rift, a network of 20 broadband seismic stations was deployed in Tanzania between June 1994 and May 1995. Data recorded by the Tanzania network have already been used to characterize crustal and uppermost mantle velocity structure beneath the network [*Last et al.*, 1997; *Brazier et al.*, 1997; *Langston et al.*, 1995]. In this paper, we investigate variations of upper mantle P and S velocities by inversion of travel times of teleseismic P and S waves. Our principal objective is to constrain the thickness of the lithosphere beneath the Tanzania Craton and to determine the extent to which it has been affected by Cenozoic tectonism.

2. Seismic P and S Travel Times

The Tanzania Broadband Seismic Network consisted of Strecheisen STS–2 and Guralp CMG–3 broadband seismic instrumentation and Reftek data recorders. Up to 20 stations were in operation at any time (Table 1). Station MTAN was reinstalled as AMBA in January 1995 because of noisy site conditions. The seismographs were deployed in two obliquely oriented arrays, transecting the Tanzania Craton from southwest to northeast and from west to east over distances of about 900 km (Figure 1). Nine of the stations were placed within the Tanzania Craton, seven stations were in the Mozambique Belt, and four were in the Ubendian Belt. The stations are separated by about 100 km. Details of this experiment are given by *Owens et al.* [1995] and *Nyblade et al.* [1996].

We analyze travel times of P and S phases generated by earthquakes at angular distances between 30° and 90° from the Tanzania network. For this distance range, P and S turn within the lower mantle, so that their ray paths are not influenced by strong velocity gradients and can be well predicted. We also use recordings of the core phases PKP and SKS which propagate along much steeper paths than P and S through the upper mantle beneath the stations.

A total of 987 events with body wave magnitudes (m_b) larger than 4.7 and 104 events with m_b larger than 5.4, which are at distances between 30° and 90° from the center of the Tanzania network, occurred while the Tanzania network was in operation (Preliminary Determination of Epicenters bulletins of the National Earthquake Information Center). Nearly all events with m_b larger than 5.4 generated P and S waveform data with sufficient signal–to–noise ratio to estimate relative travel times. From 74 events that are well distributed about Tanzania, we obtain 1192 relative P travel time measurements (1052 P, 140 PKP), and from 84 events, we obtain 1159 S travel time measurements (970 S, 189 SKS) (Figure 3). All selected events that are located east and northeast of the Tanzania network have m_b larger than 5.4. Few events with m_b larger than 5.4 occurred in Europe or at the mid-ocean ridges of the Atlantic and Indian Oceans, and thus we examined events

Table 1. Station Coordinates

Station	Latitude, °S	Longitude, °E	Elevation, km
AMBA	8.11	33.26	1.42
BASO	4.32	35.14	1.70
GOMA	4.84	29.69	0.88
HALE	5.30	38.62	0.23
INZA	5.12	30.40	0.98
KIBA	5.32	36.57	1.50
KIBE	5.38	37.48	1.00
KOMO	3.84	36.72	1.11
KOND	4.90	35.80	1.42
LONG	2.73	36.70	1.38
MBWE	4.96	34.35	1.10
MITU	6.02	34.06	1.57
MTAN	7.91	33.32	1.39
MTOR	5.25	35.40	1.10
PAND	8.98	33.24	1.25
PUGE	4.71	33.18	1.35
RUNG	6.94	33.52	1.23
SING	4.64	34.73	1.46
TARA	3.89	36.02	1.27
TUND	9.30	32.77	1.66
URAM	5.09	32.08	1.12

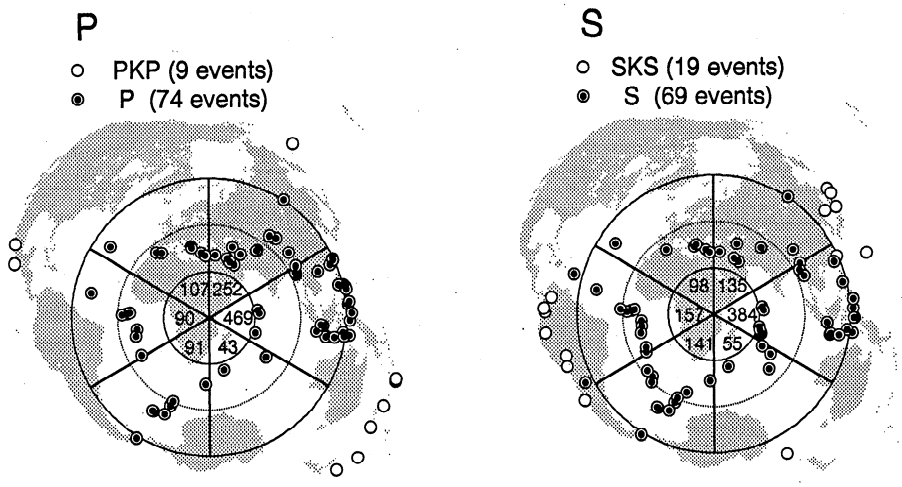

Figure 3. Epicenters of earthquakes used to estimate relative (left) P (+ PKP) and (right) S (+ SKS) travel times. PKP and SKS travel times come from events shown by the open circles. The number of relative P and S travel times obtained for events distributed in six equally wide sectors is given at the center of each plot. The large circles are at 30°, 60°, and 90° from the center of the Tanzania network.

with lower magnitudes for these regions. Only 22 of the 180 events with m_b = 4.7–5.4 that were examined produced useful S waveform data, and only 10 events produced useful P data.

The numbers plotted near the center of the maps in Figure 3 indicate the number of P and S travel time measurements made for events located in six equally wide azimuthal sectors. The distribution of measurements is not uniform primarily due to the uneven distribution of events. Nevertheless, at least 98 S and 91 P travel time measurements are available in five of the six sectors.

2.1. Measurement of Relative Travel Times

We isolate waveform segments with a duration of 200 s that are centered on the P and S arrival time. A band-pass frequency filter is applied to reduce low-frequency and microseismic noise and waveform complexity due to heterogeneous rupture. The high-pass cutoff frequency used is 25 mHz (T < 40 s). The low-pass cutoff frequency depends on event magnitude and overall signal quality and ranges from 125 to 200 mHz (T > 5–8 s) for S waves and from 300 to 500 mHz (T > 2–3 s) for P waves. For the majority of events, P and S waveform signals are pulse-like and similar at nearly all stations. Anomalous waveforms, typically observed on fewer than three recordings, are not further analyzed.

P and S travel time delays are estimated with respect to the global reference model IASP91 [*Kennett and Engdahl*, 1991] using the multichannel cross-correlation (MCCC) method of *VanDecar and Crosson* [1991]. This method exploits the waveform coherency observed across a regional network and has an advantage over conventional methods that rely on identifying first motions when wave onsets are emergent or obscured by noise. S wave onsets, in particular, cannot be easily picked in the coda of P, even for events with m_b higher than 5.5 that otherwise generate high-amplitude S waveforms.

The MCCC method consists of three steps. First, a marker is placed at a coherent waveform feature, such as the onset or peak amplitude of a wave pulse for each station i. Second, for a specified window around this marker, the maximum of the waveform cross-correlation function is computed for all possible pairs of stations i and j. This yields relative travel times: $\Delta t_{ij} = \delta T_i - \delta T_j$, where $\delta T_i = T_i^{\text{pick}} - T_i^{\text{IASP91}}$. Since noise is present in waveforms, the set of Δt_{ij} estimates are not perfectly consistent (i.e., $\Delta t_{13} \neq \Delta t_{12} + \Delta t_{23}$). In the third step of the MCCC method, a least squares optimization scheme determines slight time adjustments to the travel time delays that minimize Δt_{ij} inconsistencies. The uncertainties of relative travel times are about 0.1–0.15 s for P and 0.2–0.3 s for S. These estimates are determined from the variation of relative travel times observed when cross-correlation window lengths or band-pass filter settings are slightly changed. This uncertainty is larger than the formal standard errors that can be obtained from the MCCC method.

In Figure 4, we plot relative travel times of P and S for six events whose azimuthal patterns are representative of the entire data set. P and S travel times recorded at stations TUND and PAND, and those within the Mozambique Belt region are generally longer than those recorded at stations in the Tanzania Craton, indicating the presence of relatively low seismic velocity structure beneath the rifts. The strongest travel time variations across the Tanzania network (as large as 3–4 s for P and 7–8 s for S) are observed for events to the southwest and northeast of the Tanzania network. Much smaller travel time variations are observed for events located east of

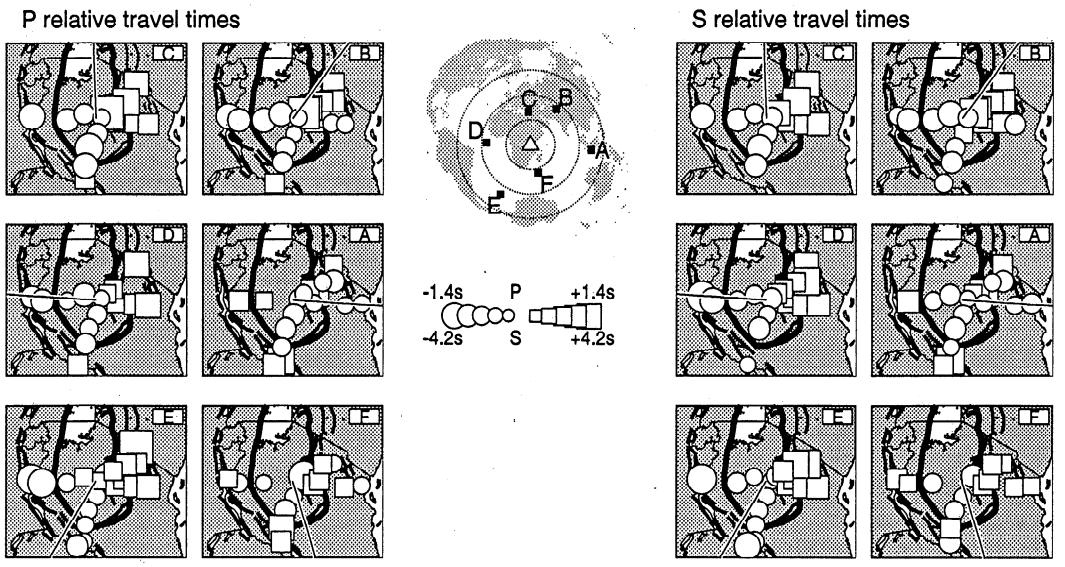

Figure 4. (left) P and (right) S relative travel times for six events at different azimuths from the Tanzania network. Circles are plotted at station locations where travel times are shorter than the network average (relative fast arrivals). Travel times longer than average are plotted by squares (relative slow arrivals). The size of the circles and squares is proportional to the magnitude of the relative travel time delays. The thin solid lines indicate the azimuth of the event relative to the stations. Geologic features correspond to those in Figure 1. The event epicenters are plotted with solid squares on a map centered on east Africa. The three dotted circles on this map are at 30°, 60°, and 90° angular distance from station MBWE.

the network. The variation of relative travel times of S waves is typically 2–3 times stronger than that for P waves, indicating that S velocity variations are approximately 1.5 times stronger than P velocity variations. The P and S travel time patterns are very similar, indicating similar P and S upper mantle velocity variations.

3. Inversion of Relative Travel Times for 3-D Seismic Velocity Structure

The relative travel times are inverted for laterally heterogeneous velocity structure using the inversion scheme developed by *VanDecar* [1991]. This routine is based in principle on the strategy first proposed by *Aki et al.* [1977] and includes some important modifications that have been developed during the past two decades. These include model parameterization using smooth functions [e.g., *Dziewonski et al.*, 1977; *VanDecar*, 1991], incorporating earthquake relocation as inversion parameters, nonlinear optimization procedures [e.g., *Paige and Saunders*, 1982], and 3–D ray tracing to compute accurate ray paths through the model [e.g., *Thomson and Gubbins*, 1982; *Koch*, 1985]. Previous applications of *VanDecar's* [1991] method have been presented by *VanDecar et al.* [1995], *VanDecar and McNamara* [1996], and *Wolfe et al.* [1997].

3.1. Model Parameterization

We parameterize the upper mantle beneath the Tanzania Seismic Network with splines under tension pinned at a series of regular knots [*Cline*, 1981]. The spline tension controls the interpolation between the knots. For example, a tension equal to zero corresponds to cubic splines, and for very large tension values (> 20), the parameterization approximates trilinear interpolation. In our application, we use a tension of 10, which allows for both smooth and localized model structures without introducing significant side-lobe artifacts (see *Neele et al.* [1993] for a detailed discussion of the splines–under–tension parameterization).

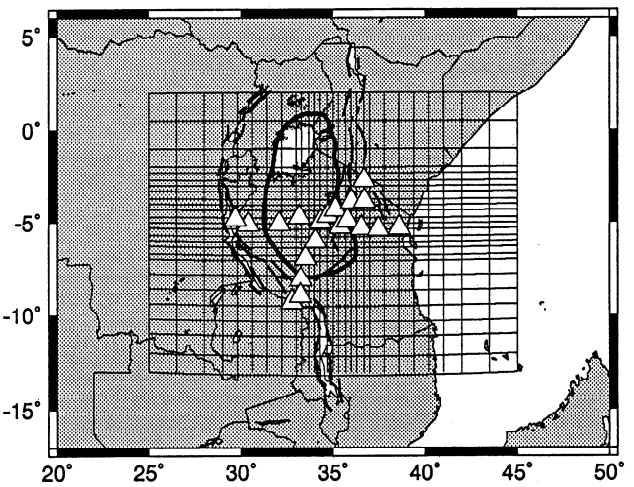

Figure 5. Lateral distribution of knot locations of the model space that is parameterized by splines under tension. The model space extends to a depth of 1000 km.

We use 34 knots in depth, 28 knots in latitude, and 29 knots in longitude amounting to a total of 27,608 knots. The grid extends from the Earth's surface to a depth of 1000 km, from latitude 13°S to 2°N, and from longitude 25°E to 45°E, extending about 4° beyond the region spanned by the stations. Between 0 and 700 km depth, knots are spaced 25 km apart. Below 700 km depth the node spacing is 50 km. The lateral knot spacing is 0.3° in the interior model region and is reduced to 1.5° between the outermost knots. The surface projection of this grid is plotted in Figure 5.

3.2. Model Sampling by Seismic Rays

It is well understood that high resolution of velocity structure can be expected only in regions that are traversed by multiple seismic rays arriving at a range of different distances and back azimuths. The accuracy of the seismic velocity model can be effectively analyzed by inversions of synthetic data sets, as discussed in section 5. It is, nonetheless, illustrative to schematically examine ray path geometry and ray density on which model resolution is primarily based.

Figure 6 displays S and SKS ray paths computed for events that are located at opposite sides of a linear array of eight stations. The stations span a distance of 8° and are separated by 1°, corresponding to the aperture and station spacing of the Tanzania network. The S rays are computed for epicentral distances of 40°, 60°, and 80°, and the SKS rays are computed for a distance of 110°. For this geometry, the highest density of crossing rays lies between 150 km and 400 km depth beneath the array. We should therefore expect maximum resolution from the inversion procedure in this depth range of the model.

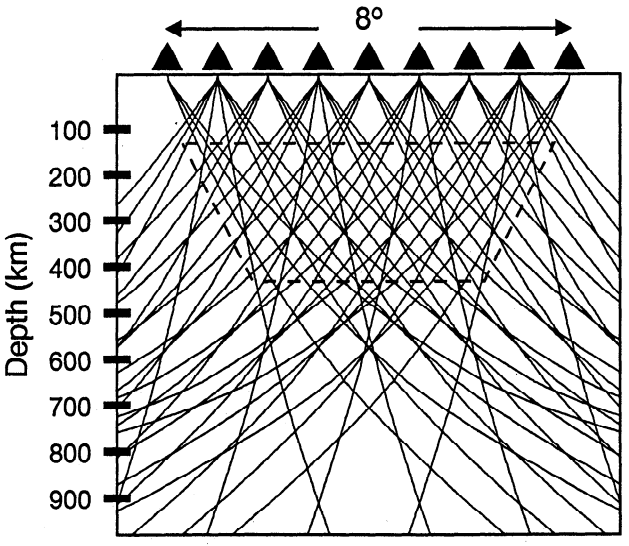

Figure 6. Schematic illustration of teleseismic ray coverage beneath a linear array of eight stations (solid triangles) with a spacing of 1°. Shown are S ray paths for epicentral distances of 40°, 60°, and 80° and SKS rays for an epicentral distance of 110°, arriving from opposite directions at the array. The region outlined by dashed lines indicate the model region with significant ray crossing and where maximum velocity model resolution is expected.

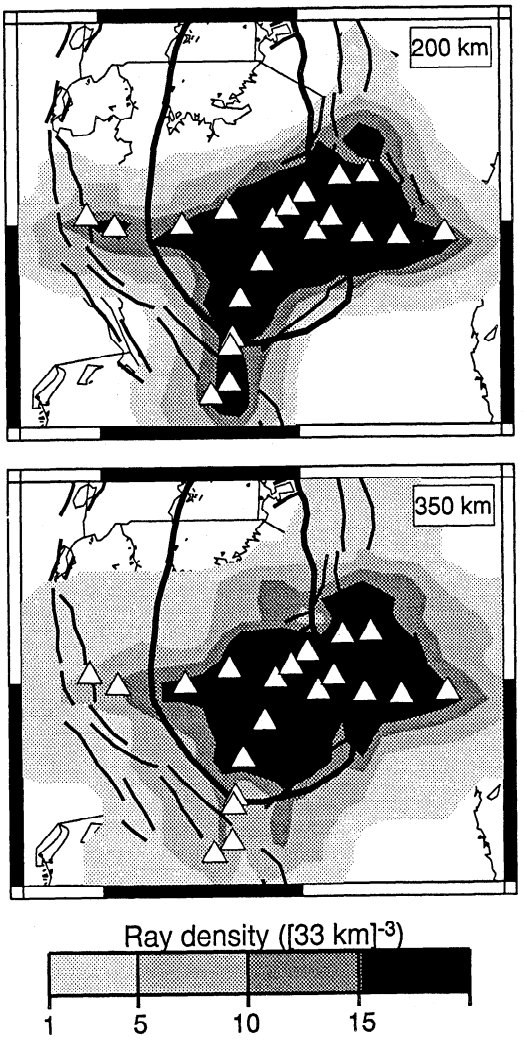

Figure 7. Ray density (per (33 km)^3) of S and SKS rays for horizontal cross sections at 200 and 350 km depth. Geologic features correspond to those in Figure 1.

In addition to the crossing of rays, ray density provides another indicator of where velocity structure is best resolved. In Figure 7, the P and S ray density for our data set is shown at 200 km and 350 km depth in our model. Ray density is highest beneath the center of the network, and regions with ray density higher than 5 correspond roughly to regions with the maximum ray crossing. Ray density is higher than 15 in the upper mantle beneath the eastern branch and the southern and southeastern regions of the Tanzania Craton, indicating where the greatest detail in velocity structure can be resolved.

3.3. Inversion Method

Relative arrival times of P ($+PKP$) and S ($+SKS$) are independently inverted for compressional and shear velocity slowness (the reciprocal of seismic velocity),

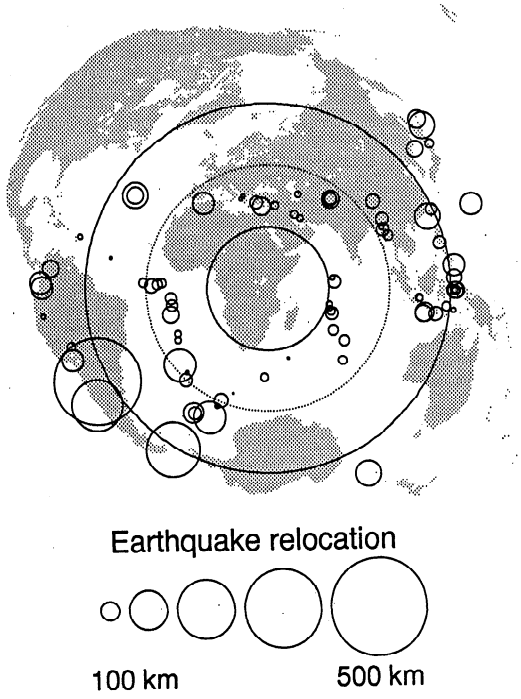

Figure 8. Magnitude of earthquake relocations applied to stabilize the travel time inversion. The size of the earthquake relocation is proportional to the size of the circle. The large circles are at 30°, 60°, and 90° from the center of the Tanzania network.

and earthquake relocations. In contrast to the study by *VanDecar et al.* [1995], we omit "station calibrations" in our inversion procedure and correct for differences in crustal structure [*Last et al.*, 1997] and station elevations explicitly. The use of station calibrations appears important only for resolving structure in the uppermost 100 km of the mantle.

Some of the strongest travel time trends are observed for earthquakes in South America and the southwest Atlantic. S travel time delays for earthquakes in these regions are anomalous and increase systematically by more than 8 s for stations at increasingly larger epicentral distance. We suspect that this trend is caused by a broad low-velocity structure in the lower mantle beneath southern Africa through which the S rays propagate (J. Ritsema et al., New seismic constraints on a large thermal upwelling beneath Africa, submitted to *Nature*, 1998). We were unsuccessful in suppressing such trends by subtracting travel time predictions made for the aspherical shear velocity model SH12_WM13 [*Su et al.*, 1994]. This is not unexpected since the S paths to stations of the Tanzania network are separated by distances much smaller than the spatial resolution ($\sim$ 3000 km) of model SH12_WM13. Rather than relying on global velocity models to correct travel time anomalies for mid mantle and lower mantle contributions, we allow the inversion to adjust the earthquake origin times and hypocentral coordinates to compensate for trends in travel time delays. Earthquake relocations obtained after the inversion are largest ($\sim$ 400 km) for the South American and southwest Atlantic events (Figure 8).

To obtain a unique solution, the inversion is regularized by searching for the model with the least amount of structure (smoothest model) required to match the data within standard errors. Structure is represented by spatial derivatives, and we seek to minimize both spatial gradient (first derivative) and model roughness (second derivative) [*Constable et al.*, 1987; *Neele et al.*, 1993; *Bostock and VanDecar*, 1995]. The minimization is conducted using a conjugate gradient procedure [*VanDecar and Snieder*, 1994]. We iterate upon these inversions by systematically downweighting equations associated with relatively large ($>$ 1.5 standard deviations) travel time residuals that persist after a previous iteration [*Egbert and Booker*, 1986]. We perform five iterations of downweighting, and each of these iterations involves 2000 conjugate gradient steps, resulting in P and S models which explain 85% and 75% of the root–mean–squared travel time residual, respectively.

4. P and S Velocity Models

Images of the laterally heterogeneous velocity models obtained from the travel time inversions are plotted in Plate 1. Four horizontal and two vertical cross sections through the P and S velocity models are shown. The horizontal cross sections are taken at depths of 100 km, 200 km, 300 km, and 400 km. The vertical cross section A–A′ and B–B′ are 8° long and displayed from 100 km to 500 km depth. Seismic velocity variations are only shown for regions of the model where ray density is at least 5 (see Figure 7).

Patterns of P and S velocity variations are very similar because of the nearly identical variation in relative P and S travel times (Figure 4). The difference in the range of P and S variations is consistent with the magnitude of P and S travel time variations. Lower–than–average seismic velocities beneath the eastern branch of the rift extend to at least 400 km depth and laterally over a distance of about 200 km. The strongest S velocity reductions ($>$ 3%) are resolved at about 100 km to 150 km depth. However, S velocity reductions of 2.5% persist to at least 400 km depth, indicating the vertical continuity of low-velocity structure within the upper mantle associated with the East African Rift. At 150 km depth, the transition from low velocities beneath the eastern branch to high velocities beneath the Tanzania Craton is fairly sharp and is located near stations SING and MTOR (see Figure 1). This transition is more diffuse at greater depth and is located at least 100 km southwest of SING and MTOR.

The seismic structure beneath the western branch is poorly constrained because, for logistic reasons, all but one of the seismic stations were located east of the western branch, and thus ray density is low. However, P and S travel time delays at TUND and PAND are as large as those at KOMO and LONG, suggesting that strong

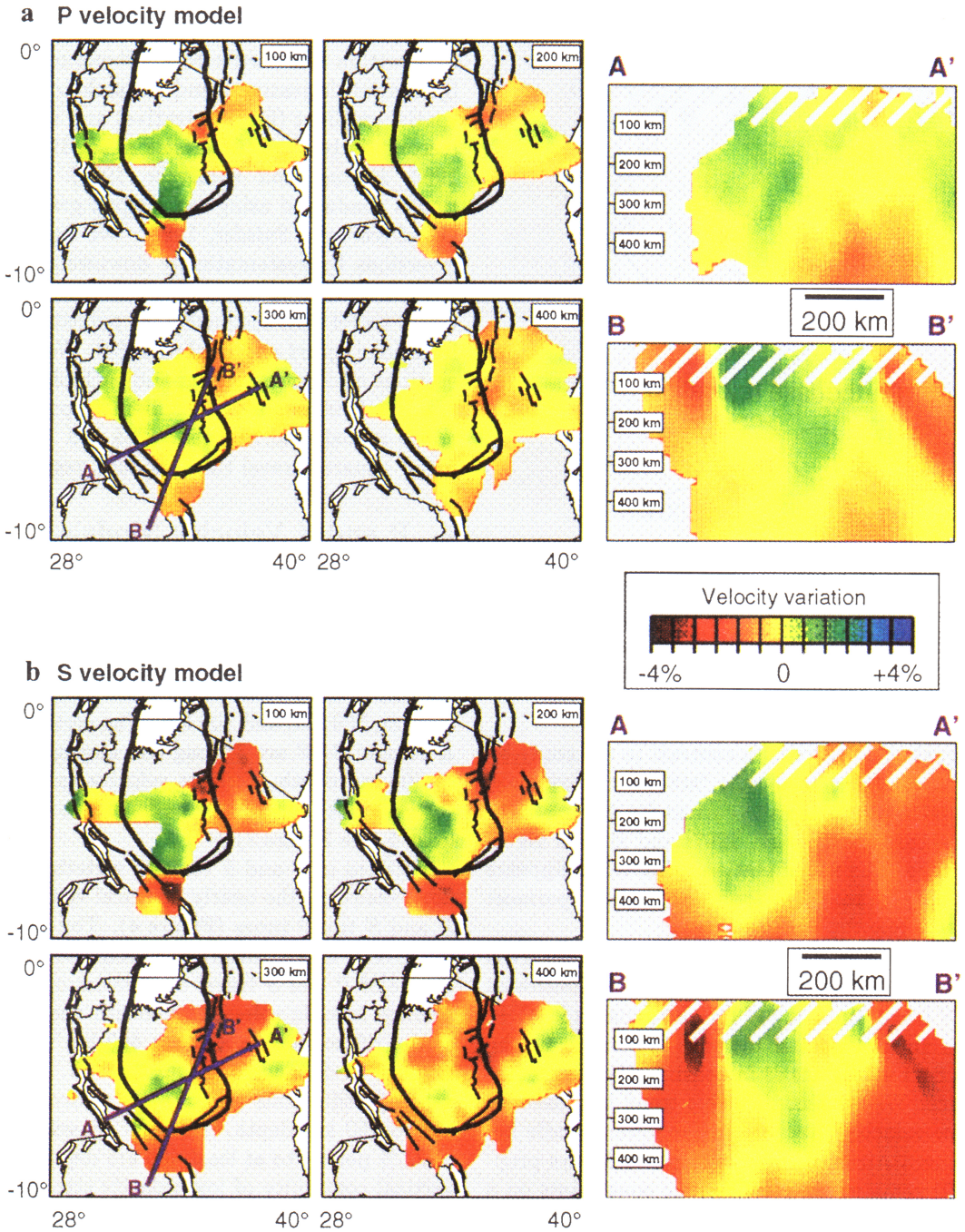

Plate 1. (top) P and (bottom) S velocity models obtained by teleseismic travel time inversion. Shown are four horizontal cross sections taken at 100 km, 200 km, 300 km, and 400 km depth. Two vertical cross sections along lines A–A′ and B–B′, whose locations are indicated in the 300–km–depth slice, are 8° long, and extend to a depth of 500 km. These cross sections are drawn without vertical exaggeration. Grey hatch marks cover the uppermost 100 km of the mantle where resolution is poor due to the lack of ray crossing (see Figure 6). The color shades represent the magnitude and polarity of the resolved seismic velocity variations: "hot" colors indicate lower–than–average seismic velocity, "cold" colors represent higher–than–average seismic velocity. The color scales for the P and S models are identical and have maximum amplitudes of 4%.

P and S velocity reductions over a large depth range exist beneath these stations also. Systematic travel times delays are also observed at GOMA and INZA, although these are generally not as anomalous as at TUND and PAND.

A slightly higher–than–average velocity is resolved for the lithosphere beneath the Tanzania Craton. At 300 km depth, patches of low S velocity structure are located well within the margins of the Tanzania Craton (as defined by geologic structures at the surface). Low-velocity regions are continuous below this depth. Nevertheless, a S velocity contrast between the craton and the eastern branch of about 5–6% persists to a depth of at least 350 km.

5. Estimates of Model Resolution

We must expect inaccuracies in the P and S models given the limited ray sampling and the regularization used to attain convergence in the inversion procedure. Various resolution limitations of our modeling procedure can be explained qualitatively. For example, abrupt velocity transitions are not easily resolved because the inversion procedure penalizes strong spatial gradients. Second, the inversion procedure projects systematic travel time delays into earthquake origin time shifts, resulting in weaker contrasts between seismic structures than may actually be present. Third, elongation and averaging of seismic velocity structure are predominantly in the vertical direction because teleseismic rays traverse the upper mantle steeply.

Since our tomographic inversion procedure does not yield a resolution matrix, we follow a common approach to estimate the extent to which artifacts from the inversion procedure may have influenced the seismic velocity models in order to identify the robust features in the seismic velocity images. In this approach, travel times are computed for a specified model of velocity structure (input model) and inverted for seismic velocity structure using identical paths, model parameterization, and inversion regularization as used in the inversion of the actual data. Because the synthetic data are noise free, the differences between the input model and the "output model", recovered from inversion of the synthetic data, represent artifacts of the modeling procedure. We use the ray geometry and the inversion parameter settings from the S model inversion in our resolution experiments.

We have experimented with a wide variety of input models (e.g., models with smooth and abrupt velocity variations, models that contain strong vertical and horizontal layering, and models with harmonic velocity variations), and they all indicate better lateral than vertical resolution of velocity variations. The strong velocity transition between the craton and the rift, for instance, can be resolved to better than 100 km (3 knot spacings) accuracy, whereas seismic structures are strongly elongated in the vertical direction, and sharp vertical velocity contrasts cannot be resolved.

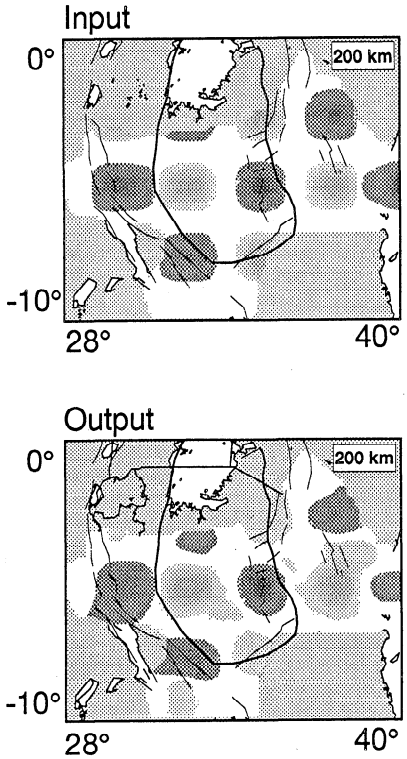

Figure 9. Illustration of lateral model resolution, using an input checkerboard model with patches of alternating low and high shear velocity structure within a 100–km–thick layer centered at 200 km depth. The output model is obtained after inversion of travel times (using the S ray geometry and S model inversion parameter settings) computed for the input structure.

The excellent lateral resolution of seismic velocity structure is demonstrated in Figure 9, which shows that a harmonic pattern of alternating low- and high-velocity patches at 200 km depth can be well resolved. The patches have a width of about 200 km, and their size and the velocity contrasts are nearly perfectly recovered. Similar results are obtained when harmonic patterns are placed at 100 km or at 400 km depth.

In the input models of Figure 10, a high-velocity craton is embedded within a low-velocity asthenosphere. The thickness of the craton ranges from 90 km to 290 km. The extreme models represent the end-member models A and B in Figures 2a and 2b. The velocity contrast between the craton and the underlying asthenosphere is 7%. Since the presence of a sharp vertical velocity gradient between the craton and the underlying asthenosphere leads to strong modeling artifacts, the resolution experiments of Figure 10 provide a minimum estimate of model resolution.

From the comparison of input and output models, the limited vertical resolution and loss of amplitude of velocity contrasts are obvious. The sharp transition of

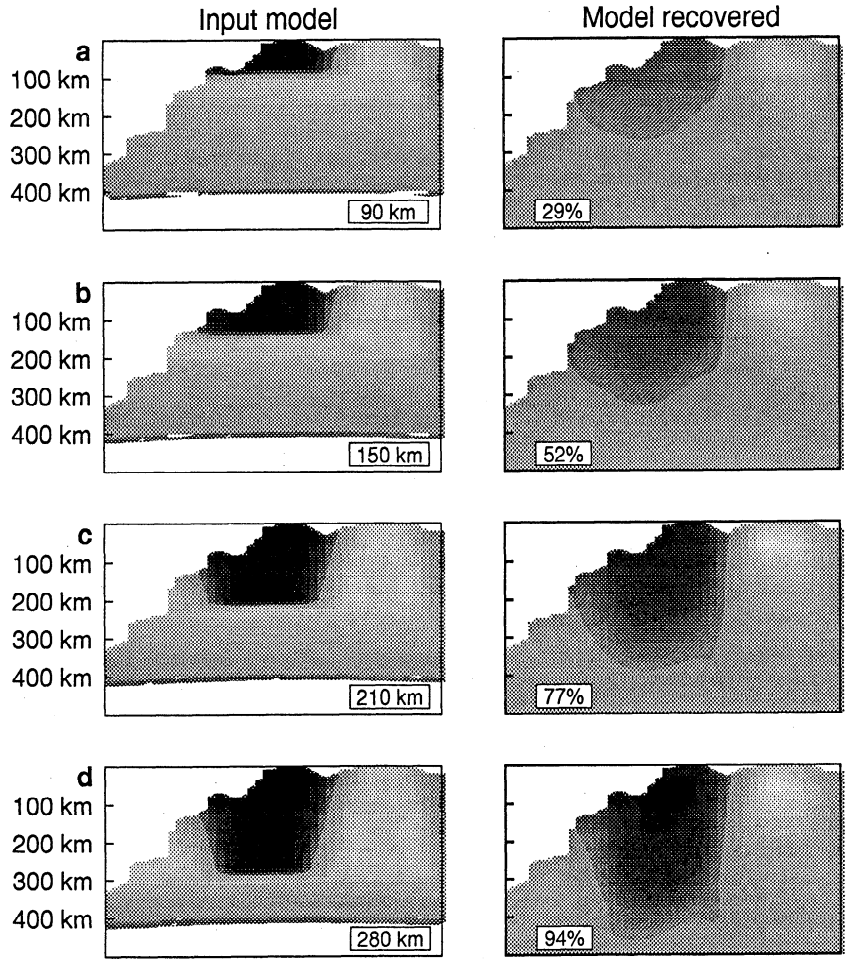

Figure 10. Illustration of vertical model resolution. (right) Seismic velocity models obtained after inversion of travel times (using the S ray geometry and S inversion parameters) computed for (left) the input structure. Cross sections through the input and output models are along A–A′, as defined in Plate 1. Models contain high-velocity (+4%) cratons embedded within a low-velocity (up to -3%) asthenosphere. The thickness of the cratons in the input models is indicated in the lower right corner. The number plotted in the lower left corner of the output models corresponds to the relative amplitude of velocity contrasts that is recovered.

velocity from the bottom of the craton to the top of the asthenosphere is not recovered, and the craton in the output models is about 100 km thicker than in the input models. Seismic structures with a vertical scale length less than 150 km are not resolvable. The recovery of the amplitude of the velocity contrast between the craton and the asthenosphere is larger than 75% only for models with a craton that is thicker than 210 km.

6. Discussion

In evaluating to what extent the lithosphere beneath the Tanzania Craton has been modified by Cenozoic tectonism, it is necessary to make assumptions of its structure before extensional processes commenced. An obvious approach to establish the prerift structure of the Tanzania Craton is to use models of cratonic lithosphere elsewhere. However, the precise thickness of cratons in other regions of the world remains controversial, with minimum estimates of around 200 km and maximum estimates of 400 km or more, so this approach is not necessarily simple.

Recent estimates of maximum thickness originate primarily from seismic tomography [e.g., *Grand*, 1994; *Trampert and Woodhouse*, 1996; *Zhang and Lay*, 1996; *Ekström et al.*, 1997; *Van der Lee and Nolet*, 1997]. Establishing the thickness of continental lithosphere from the seismic models is not always straightforward because low-velocity zones within the upper mantle beneath continents are generally not well developed or easily identified. Thermobarometry studies of prerift African mantle xenoliths provide a less ambiguous estimates of minimum lithospheric thickness because they show that superadiabatic temperature gradients continue to depths of at least 200 km [e.g., *Boyd et al.*, 1985; *Boyd and Gurney*, 1986]. Thus we assume "nor-

mal" cratonic lithosphere to be at least 200 km thick, and we define the thickness of the cratonic lithosphere in end-member model B of Figure 2b to be no less than 200 km and the thickness of the lithosphere in end-member model A of Figure 2a to be substantially less than 200 km.

The seismic images of P and S velocity variations reveal higher–than–average seismic velocities beneath the Tanzania Craton that extend well below a depth of 300 km (Plate 1). Since the resolution experiments of Figure 10 indicate that vertical elongation of structures due to the inversion procedure is of the order of 100 km, we conclude that the cratonic lithosphere beneath the Tanzania Craton is at least 200 km thick. Therefore we rule out end-member model A in Figure 2a that depicts complete destruction of the cratonic keel. Based on the assumption of a prerifting thickness of about 200 km, we conclude that the cratonic lithosphere is tectonically "stable" to the extent that it has not been completely destroyed by extensional tectonics that has altered the younger surrounding mobile belt lithosphere. This conclusion is supported by recent studies of mantle xenoliths from the Tertiary Labait volcano in northeastern Tanzania, which lies on the eastern edge of the Tanzania Craton. Thermobarometry results indicate craton-like cool temperatures at depths of 150–200 km at this location, and *Re–Os* dates yield minimum ages for the xenoliths of about 2.8 Ga [*Rudnick et al.*, 1994; *Chesley and Rudnick*, 1996]. A relatively thick (> 200 km) cratonic lithosphere is also consistent with the low heat flow from the Craton [e.g., *Nyblade et al.*, 1990; *Nyblade*, 1997] and with estimates of elastic plate thickness from the gravity field [*Ebinger et al.*, 1989].

We resolve a shear velocity contrast between the cratonic lithosphere and the uppermost mantle beneath the eastern branch of the rift system of about 5–6%, but from resolution experiments, we infer that this contrast could be underestimated by as much as a factor of 1.5. Based on tomographic images of other Archean cratons showing up to 3% velocity contrasts between Archean and younger mantle lithosphere [e.g., *Grand*, 1994; *Van der Lee and Nolet*, 1997], we infer that about half of the velocity contrast ($\sim$ 2–3%) between the craton and the mobile belts results from the depleted composition of the cratonic keel. The remaining 2–3% of the velocity contrast is likely due to thermally perturbed upper mantle beneath the rifts.

In addition to improving our understanding of cratonic structure, the tomography images shown in Plate 1 have important implications for at least two tectonic issues related to the development of the rift valleys and plateau uplift. The issues are discussed very briefly here and are the focus of our continuing research. As mentioned in section 1, the cause of the rifting and associated thermal modification of the lithosphere in east Africa has been attributed by many to the presence of one or more mantle plumes. In particular, the notion that a mantle plume beneath the center of the East African Plateau gives rise to plateau uplift and rifting has received considerable attention recently [e.g., *Prodehl et al.*, 1994, and references therein; *Burke*, 1996]. Our seismic velocity images do not provide evidence for a plume-like structure beneath the Tanzania Craton shallower than 300 km depth. Below 400 km depth, areas of low-velocity structure are prevalent. However, model resolution at this depth range is limited to a narrow region beneath the center of the seismic network (Figure 6). Thus, while our models can be used to rule out the presence of a plume at depths shallower than about 300 km, they cannot be used to rule out the possibility of a plume residing beneath east Africa at depths greater than about 300 km.

The second tectonic issue relates to an old debate about the role preexisting structures have played in the localization of rift faulting in east Africa (see *Mohr* [1982] and *McConnell* [1972] for reviews). Since the lithospheric keel of the Tanzania Craton has not been disrupted to any great extent by the Cenozoic tectonism, it seems obvious that a first-order structural control on rift development in east Africa has been the thick, cold (i.e., strong) lithosphere of the craton lying within a broad region experiencing east-west extension. Because of the location of the craton in the middle of east Africa, the rift valleys have simply circumvented the thicker, colder cratonic lithosphere and developed in the thinner, warmer mobile belt lithosphere surrounding the craton.

7. Conclusions

Images of seismic P and S velocity variations obtained by inversion of teleseismic travel times recorded by the Tanzania Seismic Network indicate that the Tanzania Craton is underlain by high-velocity lithosphere with a thickness of at least 200 km. Because of the relatively limited vertical resolution of the inversion procedure, the cratonic lithosphere could be as thick as 300 to 350 km. The cratonic keel does not, however, extend deeper than that, since at depths of around 400 km the craton is underlain by substantially lower velocities. The mantle lithosphere of the craton is surrounded by anomalously low (< -3%) shear velocity structure associated with the eastern African rifts. The low-velocity structures beneath the rifts extend to depths of 300 km or more.

From our models, we conclude that the mantle lithosphere beneath the Tanzania Craton has not been extensively altered by the Cenozoic tectonism in east Africa. Thus the cratonic keel in east Africa appears to be tectonically stable, a finding which corroborates the assertion of cratonic stability described in section 1. A thick, cold lithosphere beneath the Tanzania Craton is consistent with the low heat flow from the craton and estimates of elastic plate thickness.

The elevation of the Tanzania Craton within the East African Plateau and the low Bouguer gravity anomaly

over the craton can be reconciled with our seismic models if buoyant (isostatic and/or dynamic) support is provided by hot, low-density material beneath the craton. Possibly, such hot material is associated with a mantle plume deeper within the mantle that also feeds the east African rifts.

Acknowledgments. Superb logistical support in the field was provided by P. Ngereja, C. Moshy, and A. Tesha of the Tanzania Geological Survey (Ministry of Energy and Minerals). We thank Robert Busby, Philip Crotwell, John Hammer, and Robert Last for helping with the field deployment and network maintenance. Rick Benson and Anh Ngo of IRIS/DMC assisted us with the processing of our data. We thank Cindy Ebinger, Roberta Rudnick, Ray Russo, and Philip Slack for helpful comments. All figures were generated with the GMT software of *Wessel and Smith* [1991]. This research is funded under NSF grants EAR–9304555 and EAR–9304657 and contract F49620-94-1-0066 from the Air Force Office of Scientific Research.

References

Aki, K., A. Christoffersson, and E. Husebye, Determination of the three-dimensional seismic structure of the lithosphere, *J. Geophys. Res.*, *82*, 277–296, 1977.

Bostock, M. G., and J. C. VanDecar, Upper mantle structure of the northern Cascadia subduction zone, *Can. J. Earth Sci.*, *32*, 1–12, 1995.

Boyd F. R., and J. J. Gurney, Diamonds and the African lithosphere, *Nature*, *232*, 472–477, 1986.

Boyd, F. R., J. J. Gurney, and S. H. Richardson, Evidence for 150–200 km thick Archean lithosphere from diamond inclusion thermobarometry, *Nature*, *315*, 387–389, 1985.

Brazier, R. A. Nyblade, C. Langston, and T. Owens, P_n tomography of a nascent rift, northeastern Tanzania, *Eos Trans. AGU*, Spring Meeting Suppl., 211, 1997.

Burke, K., The African Plate, *S. Afr. J. Geol.*, *99*, 341–410, 1996.

Chesley, J., and R. Rudnick, Growth and modification of the Tanzanian lithospheric mantle: preliminary Re–Os results, *J. Conf. Abstr.*, *1*, 105, 1996.

Cline, A. K., FITPACK–Software package for curve and surface fitting employing splines under tension, Dep. of Comput. Sci., Univ. of Tex. at Austin, 1981.

Constable, S. C., R. L. Parker, and C. G. Constable, Occams inversion–A practical algorithm for generating smooth models from electromagnetic sounding data, *Geophysics*, *52*, 289–300, 1987.

Dziewonski, A. M., B. H. Hager, and R. J. O'Connell, Large-scale heterogeneities in the lower mantle, *J. Geophys. Res.*, *82*, 239–255, 1977.

Ebinger, C. J., T. D. Bechtel, D. W. Forsyth, and C. O. Bowin, Effective elastic plate thickness beneath the East African and Afar Plateaus and dynamic compensation of the uplifts, *J. Geophys. Res.*, *94*, 2883–2901, 1989.

Egbert, G. D., and J. R. Booker, Robust estimation of geomagnetic transfer functions, *Geophys. J. R. Astron. Soc.*, *87*, 173–194, 1986.

Ekström, G., J. Tromp, and E. W. F. Larson, Measurements and global models of surface wave propagation, *J. Geophys. Res.*, *102*, 8137–8157, 1997.

Girdler, R. W., J. D. Fairhead, R. C. Searle, and W. T. C. Sowerbutts, The evolution of rifting in Africa, *Nature*, *224*, 1178–1182, 1969.

Grand, S. P., Mantle shear structure beneath the Americas and surrounding oceans, *J. Geophys. Res.*, *99*, 11,591–11,621, 1994.

Jordan, T. H., Composition and development of the continental tectosphere, *Nature*, *274*, 544–548, 1978.

Jordan, T. H., Structure and formation of the continental tectosphere, *J. Petrol.*, Special Lithosphere Issue, 11–37, 1988.

Kennett, B. L. N., and E. R. Engdahl, Travel times for global earthquake location and phase identification, *Geophys. J. Int.*, *105*, 429–465, 1991.

Koch, M., A numerical study on the determination of the three-dimensional structure of the lithosphere by linear and non-linear inversion of teleseismic travel times, *Geophys. J. R. Astron. Soc.*, *80*, 73–95, 1985.

Langston, C., A. Nyblade, and T. Owens, Regional earthquakes recorded by the Tanzania broadband PASSCAL experiment, *Eos Trans. AGU*, *76*, Fall Meeting Suppl., F607, 1995.

Last, R. J., A. A. Nyblade, C. A. Langston, and T. J. Owens, Crustal structure of the East African Plateau from receiver functions and Rayleigh wave phase velocities, *J. Geophys. Res.*, *102*, 24,469–24,483, 1997.

McConnell, R. B., Geological development of the rift system of eastern Africa, *Geol. Soc. Am. Bull.*, *83*, 2549–2572, 1972.

Mohr, P., Musings on continental rifts, in *Continental and Oceanic rifts*, *Geodyn. Ser.*, vol. 8, edited by G. Palmason, pp. 293–309, AGU, Washington, D.C., 1982.

Neele F., J. C. VanDecar, and R. Snieder, The use of *P* wave amplitude data in a joint inversion with travel times for upper mantle velocity structure, *J. Geophys. Res.*, *98*, 12,033–12,054, 1993.

Nolet, G., and S. Müller, A model for the deep structure of the East African Rift system from simultaneous inversion of teleseismic data, *Tectonophysics*, *84*, 151–178, 1982.

Nyblade, A. A., Heat flow across the East African Plateau, *Geophys. Res. Lett.*, *24*, 2083–2086, 1997.

Nyblade, A. A., and S. W. Robinson, The African Superswell, *Geophys. Res. Lett.*, *21*, 765–768, 1994.

Nyblade A. A., H. N. Pollack, D. L. Jones, F. Podmore, and M. Mushayandebvu, Terrestrial heat flow in east and southern Africa, *J. Geophys. Res.*, *95*, 17,371–17,384, 1990.

Nyblade A. A., C. Birt, C. A. Langston, T. J. Owens, and R. J. Last, Seismic experiment reveals rifting of craton in Tanzania, *Eos Trans. AGU*, *77*, 517, 520–521, 1996.

Owens, T. J., A. A. Nyblade, and C. A. Langston, The Tanzania broadband experiment, *IRIS News Lett.*, *XIV*, 1, 1995.

Paige C. C., and M. A. Saunders, LSQR: An algorithm for sparse linear equations and sparse least squares, *ACM Trans. Math. Software*, *8*, 43–71, 1982.

Prodehl, C., G. R. Keller, and M. A. Kahn, Crustal and upper mantle structure of the Kenya Rift, *Tectonophysics*, *236*, 483, 1994.

Rudnick, R. L., W. F. McDonough, and A. Oprin, Northern Tanzania peridotite xenoliths: A comparison with Kaapvaal peridotites and inferences on metasomatic interactions, in *Related Rocks and Mantle Xenoliths*, vol. 1, edited by H. O. A. Meyer and O. Leonardos, pp. 336–353, C.P.R.M., Brasilia, 1994.

Su, W.-J., R. L. Woodward, and A. M. Dziewonski, Degree 12 model of shear velocity heterogeneity in the mantle, *J. Geophys. Res.*, *99*, 6945–6980, 1994.

Thomson, C. J., and D. Gubbins, Three dimensional lithospheric modeling at NORSAR: Linearity of the method and amplitude variations from the anomalies, *Geophys. J. R. Astron. Soc.*, *71*, 1–36, 1982.

Trampert, J., and J. H. Woodhouse, Global phase velocity maps of Love and Rayleigh waves between 40 and 150 seconds, *Geophys. J. Int.*, *122*, 675–690, 1996.

VanDecar J. C. Upper mantle structure of the Cascadia subduction zone from non-linear teleseismic travel time inversion, Ph.D. thesis, Univ. of Wash., Seattle, 1991.

VanDecar J. C., and R. S. Crosson, Determination of teleseismic relative phase arrival times using multi-channel cross-correlation and least-squares, *Bull. Seismol. Soc. Am.*, *80*, 150–169, 1991.

VanDecar J. C., and D. McNamara, Three-dimensional upper mantle velocity structure beneath the Tibetan Plateau, *Eos* Trans. AGU, *77* (46), Fall Meet. Suppl., F694, 1996.

VanDecar J. C., and R. Snieder, Obtaining smooth solutions to large, linear inverse problems, *Geophysics*, *59*, 818–829, 1994.

VanDecar J. C., D. E. James, and M. Assumpção, Seismic evidence for a fossil mantle plume beneath South America and implication for plate driving forces, *Nature*, *378*, 25–31, 1995.

Van der Lee, S., and G. Nolet, Upper mantle S velocity structure of North America, *J. Geophys. Res.*, *102*, 22,815–22,838, 1997.

Wessel, P., and W. H. F. Smith, Free software helps map and display data, *Eos Trans. AGU*, *72*, 441, 445–446, 1991.

Wohlenberg, J., The structure of the lithosphere beneath the East African Rift zones from interpretation of Bouguer anomalies, in *Afar Depression of Ethiopia*, vol. 2, pp. 125–130, edited by A. Pilger, and S. Rosler, Schweitzerbart, Stuttgart, Germany, 1975.

Wolfe, C. J., I. T. Bjarnason, J. C. VanDecar, and S. C. Solomon, Seismic structure of the Iceland mantle plume, *Nature*, *385*, 245–247, 1997.

Zhang, Y.-S., and T. Lay, Global surface wave velocity variations, *J. Geophys. Res.*, *101*, 8415–8436, 1996.

C. A. Langston and A. A. Nyblade, Department of Geosciences, Pennsylvania State University, University Park, PA 16802. (e-mail: cal@essc.psu.edu; andy@essc.psu.edu)

T. J. Owens, Department of Geological Sciences, University of South Carolina, Columbia, SC 29208. (e-mail: owens@sc.edu)

J. Ritsema, Seismological Laboratory, California Institute of Technology, Pasadena CA 91125. (e-mail: jeroen@takkie.gps.caltech.edu)

J. C. VanDecar, Department of Terrestrial Magnetism, Carnegie Institution of Washington, 5241 Broad Branch Road N.W., Washington, DC 20015. (e-mail: vandecar@dtm.ciw.edu)

(Received October 27, 1997; revised March 6, 1998; accepted April 8, 1998.)